PROCEEDINGS OF SCIENCE

Feasibility of Anisotropic Flow measurements at NICA/MPD

N. S. Geraksiev* **for the MPD collaboration**

FPET, Plovdiv University "Paisii Hilendarski", Plovdiv, Bulgaria
VBLHEP, Joint Institute for Nuclear Research, Dubna, Russia

E-mail: nikolay.geraksiev@gmail.com

Anisotropic flow is a key observable in heavy ion collisions. In the presented article a short introduction to the proposed NICA/MPD project is given, as well as measurements concerning elliptic flow of identified hadrons (p, π, K, Λ) from simulated and reconstructed UrQMD events.

XXII International Baldin Seminar on High Energy Physics Problems,
15-20 September 2014
JINR, Dubna, Russia

*Speaker.

PoS(Baldin ISHEPP XXII)131

1. Introduction

1.1 Nuclotron-based Ion Collider fAcility (NICA)

Investigation of the hot and dense baryonic matter is currently an exciting field in modern high energy physics. Besides being crucial to a better understanding of the early stages of the Universe and the formation of neutron stars, it is useful for the comprehension of in-medium properties of hadrons and nuclear matter equation of state, and may prove to be a means of search for manifestations of deconfinement and/or chiral symmetry restoration.

The Nuclotron upgrade, which is a substantial part of the JINR scientific program, is dedicated to the investigation of hot and dense baryonic matter. The Nuclotron-based Ion Collider fAcility (NICA) will create Au+Au collisions over a wide range of atomic masses, at a centre-of-mass energy of $\sqrt{s_{NN}} = 11$A GeV (for Au^{79+}) and an average luminosity of $L = 10^{27}\text{cm}^{-2}\text{s}^{-1}$, proton-proton collisions with $\sqrt{s_{pp}}$ =26A GeV and $L = 10^{30}\text{cm}^{-2}\text{s}^{-1}$.

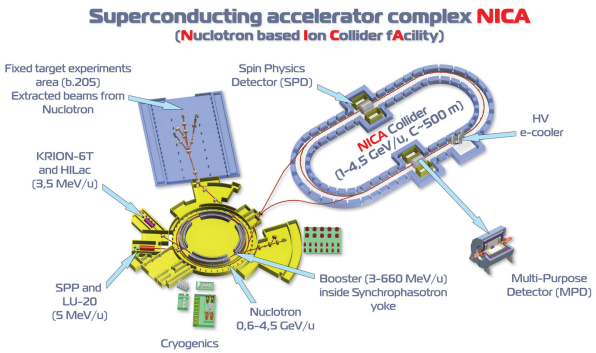

Figure 1: The NICA accelerator complex at JINR

Along with the heavy ion programme, the NICA facility will provide proton and light ion beams, and the possibility to obtain and utilize unique polarized beams. This holds a great potential for studies of the nuclear quark-gluon structure in processes with large momentum transfer, as well as in measurements with target/projectile polarization, and research on experimental verification of quark counting rules, clarification of the abnormal behavior known as color nuclear transparency, as well as comprehension of large spin effects in production of mesons and hyperons.

The accelerator will also allow collisions of mass-asymmetric beams including *pA* collisions. In and of itself an interesting field, it is also quite important as a reference point for comparison with heavy ion data. Furthermore, as a long-term goal, the accelerator facility may provide electron-ion collisions for measurements of nucleon and nuclei electro-magnetic form factors to large momenta, *e.g.* investigation of spatial distributions of charge and magnetization in nuclei and the nucleon including the determination of the valence quark generalized parton distribution, revealing the correlation between spatial and momentum distributions.

It should be noted that while the NICA project is aimed at fundamental scientific research, other applications of the particle beams such as biomedical research and radiation technology have been planned [1, 2].

1.2 MultiPurpose Detector (MPD)

The NICA collider is going to have two interaction points, allowing for two detectors to operate simultaneously. The MultiPurpose Detector (MPD) is one of these detectors. In the first stage of the NICA/MPD project are considered analyses on multiplicity and spectral characteristics of identified hadrons including strange particles, multi-strange baryons and antibaryons, characterizing entropy production and system temperature at freeze-out. Moreover, event-by-event fluctuations in multiplicity, charges, transverse momenta and K/π ratios are to be studied as a generic property of critical phenomena, along with collective flow effects, HBT correlation, and femtoscopy. In the second stage measurements of the electromagnetic probes (photons and dileptons) will be carried out. The MPD detector will be operated at a rate of about $7 \cdot 10^3$ interactions per second, with multiplicities of up to ~ 1500 charged particles per central gold-gold collision at maximal energy of $\sqrt{s_{NN}} = 11$A GeV [1, 2, 3].

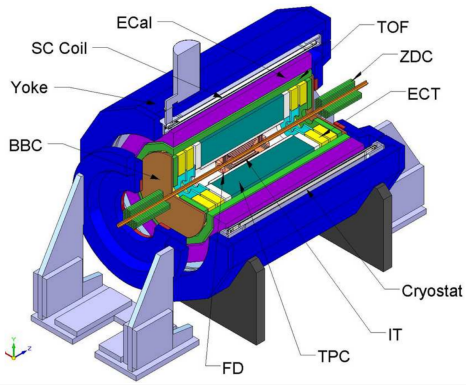

Figure 2: Central part of the MultiPurpose Detector

The design of the detector requires a very low material budget as the average transverse momentum of the particles produced in a collision at NICA energies is below 500 MeV/c.

The barrel part, consisting of a tracker and particle identification system is shown in Fig.(2). The time projection chamber (TPC) is the principal tracker yielding precise track finding, momentum determination, vertex reconstruction and pattern recognition up to $|\eta| < 2$ .The energy loss (dE/dx) measurements in the TPC gas will provide an additional capability for particle identification in the low momentum region [5].

The high performance time-of-flight (TOF) system must be able to identify charged hadrons and nuclear clusters in the broad rapidity range and up to total momentum of 2 GeV/c. The TOF detector covers $|\eta| < 3$ and its performance should allow the separation of kaons from protons up to a total momentum of 3 GeV/c [6].

Fast timing and triggering is performed by arrays of quartz counters (FD). The forward going energy for centrality selection and event plane reconstruction will be measured by to sets of hadron calorimeters (ZDC), covering the pseudorapidity region $2.5 < |\eta| < 4$ [7].

The main aim of the electromagnetic calorimeter (EMC) is identification of electrons and photons, and high precision measurements of their energy. The high granularity, excellent energy resolution and good timing performances of the EMC will enhance the overall efficiency and particle identification capabilities of the MPD detector [3, 4].

2. Anisotropic Flow

Measurements of collective flow phenomena are crucial tools for the study of properties in the dense matter created in relativistic heavy ion collisions (such as the equation of state - EOS, formation conditions, *etc.*). The physics dynamics at the early stages of non-central heavy ion collisions is assessed by the azimuthal anisotropy of particle production with respect to the reaction plane [11]. The reaction plane is defined by the impact parameter and the beam direction z. The

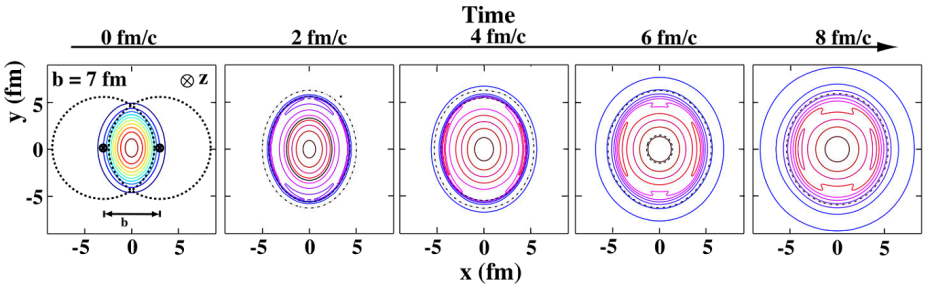

Figure 3: Evolution of the transverse energy density profle in coordinate space for non-central heavy ion collisions

Fourier expansion of the invariant triple differential distributions proves to be a convenient way of characterizing the various patterns of anisotropic flow:

$$E\frac{\mathrm{d}^3N}{\mathrm{d}^3\mathbf{p}} = \frac{\mathrm{d}N}{p_T\mathrm{d}p_T\mathrm{d}\phi\mathrm{d}y} = \frac{1}{2\pi}\frac{\mathrm{d}N}{p_T\mathrm{d}p_T\mathrm{d}y}\left(1+2\sum_{n=1}^{\infty}v_n\cos(n(\phi-\Psi_{RP}))\right), \tag{2.1}$$

where E is the energy of the particle, $\mathbf{p}$ the momentum, p_T the transverse momentum, ϕ the azimuthal angle, y the rapidity, and Ψ_{RP} the reaction plane angle. The sine terms in such an expansion vanish because of the reflection symmetry with respect to the reaction plane. The Fourier coefficients are p_T and y dependent and are given by

$$v_n(p_T,y) = \langle\cos(n(\phi-\Psi_{RP})\rangle \tag{2.2}$$

where the angular brackets denote an average over the particles summed over all events in the (p_T, y) bin under study. Fig. (3) depicts the evolution of the almond shaped interaction volume. Plots from left to right show how the system evolves from an almond shaped transverse overlap region into an almost symmetric system and contours indicate the energy density profile. During this expansion, governed by the velocity of sound, the created hot and dense system cools down[11].

The coefficient v_1 is also known as directed flow and it presents a means of measuring the total amount of transverse flow. It is most pronounced in the cases of semi-central interactions around target and projectile rapidities where the spectators are deflected away from the beam axis due to a bounce-off from the compressed and heated matter in the overlap region.

The elliptic flow is paid special attention as this collective motion is formed mainly at an early stage of the collision. According to the typical hydrodynamic scenario, the $v_2(p_T)$ values at relatively low transverse momenta ($p_T < 2$ GeV/c) are determined mainly by the internal pressure gradients of the expanding fireball during the initial high density phase of the reaction. The elliptic

flow of hadrons at low transverse momenta can be related to the degree of thermalization, viscosity, and EoS of the produced matter. However, the elliptic flow of the high momentum particles is related to the jet fragmentation and energy loss of the primordially produced hard antiquark-quark pair traveling through the hot QCD medium. At moderate p_T the experimental data indicate a gradual increase of v_2 with p_T. A deeper insight into the bulk properties of the produced matter is obtained by an accurate v_2 mesurement.

Two main reasons justify the increased demand for an accurate study of (anti)hyperon production. Firstly, a signature for deconfinement might be manifested by strangeness enhancement in heavy-ion collisions relative to proton induced reaction[12, 13, 14]. Secondly, due to the small hadronic cross-sections of multi-strange hyperons, additional rescaterring effects in the dense hadronic matter for strange hadrons are not as significant as compared to other hadrons. Therefore, measurements of phase-space distributions of strange hyperons reveal key characteristics of the fireball at the early stages of the system evolution. Moreover, it has recently been observed by the STAR experiment that the characteristic azimuthal anisotropy pattern (*e.g.* the elliptic flow coefficient v_2 as a function of transverse momemtum p_T) for anti-baryons is different from the one for baryons in midcentral Au+Au collisions at energies $\sqrt{s_{NN}} < 11$A GeV [15]. There is interplay between particle production and subsequent absorption in the medium meaning that anti-baryons are strongly affected by the co-moving baryon density in the course of the reaction. Different values of the collision energy and beam atomic mass number at NICA will provide a valuable insight into the reaction dynamics on (anti)hyperon production.

3. Analysis and Results

The analysis procedure was carried out using the MPDroot software (based on FairRoot) and the flow analysis package used by the STAR and ALICE experiments. Events were generated with the UrQMD 3.3 model, commonly used in heavy ion research [16, 17]. A total of 3.10^5 gold-gold (Au^{79+}) collisions with impact parameter in the range of $0-9$ fm and energy $\sqrt{s_{NN}} = 11$A GeV were analyzed. The produced particles were transported through the TPC and TOF detectors using the GEANT3 transport package [21]. Tracks were reconstructed with the Kalman filtering technique [22]. In order to achieve a good precision of momentum and energy loss measurements, a track selection criteria of minimum 10 TPC points was required. The full range of TPC pseudorapidity was used ($|\eta| < 2$). The reconstructed TPC tracks were extrapolated to the TOF detector and matched to TOF hits.

Several particle identification methods are available for the MPD experiment. For this particular study the Bayesian approach based on energy loss dE/dx from TPC and TOF M^2 information was used (see [23]) to differentiate between track candidates' probabilities to be of certain particle species. For the elliptic flow study identification of charged hadrons (p, π, K) was done in terms of highest probability *e.g.* if the track has the highest probability value to be that of a proton than say pion, we regard the track as to be that of a proton. A selection criteria threshold was introduced so that only tracks above a certain probability P_{trust} may be tagged. Particle identification quality was estimated (see Fig. (4) and Tab. (1)) by efficiency and contamination as functions of transverse momentum:

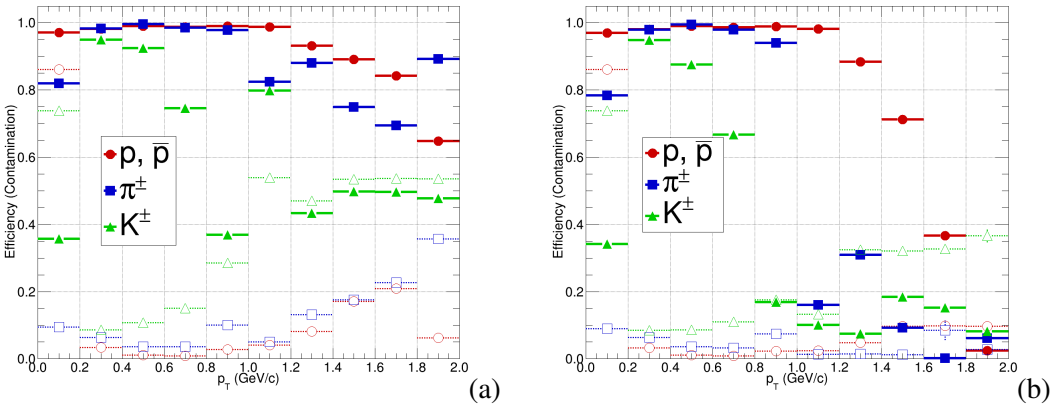

Figure 4: Particle identification efficiency and contamination as a function of transverse momentum for probability thresholds of (a) - $P_{trust} > 0$ and (b) - $P_{trust} > 0.6$

Particle	**p, $\bar{\text{p}}$**	**$\pi^{\pm}$**	**$\text{K}^{\pm}$**
$\text{P}_{\text{trust}} > 0$			
Efficiency, %	90.84	91.48	66.01
Contamination, %	22.92	7.25	43.76
$\text{P}_{\text{trust}} > 0.6$			
Efficiency, %	82.41	83.62	47.41
Contamination, %	19.48	5.82	26.70

Table 1: Particle identification efficiency and contamination

$$E^i = \frac{N^i_{corr}}{N^i_{ana}}, \; C^i = \frac{N^i_{incorr}}{N^i_{Ncorr} + N^i_{incorr}} \tag{3.1}$$

where E^i and C^i are the efficiency and contamination of a particle species i, N^i_{corr} is the number of correctly identified particles, N^i_{ana} - the number of generated particles with more than 10 points in TPC and N^i_{incorr} is the number of incorrectly identified particles.

It should be noted that particle identification plays a key role in elliptic flow determination and while the purpose of this study was not particle identification itself, the optimization of the identification criteria is to be carried out in subsequent studies.

3.1 Event Plane Angle

A well established method of analysing the anisotropic flow is given in [18] [19]. The event plane angle was reconstructed by all identified charged tracks ($P_{trust} \geq 0$) using two sub-events in negative and positive rapidity. The tracks in these sub-selections build sub-Q vectors from which two sub-event plane angles are then determined:

$$\Psi_n = \frac{1}{n} \arctan\left(\frac{\sum w_i \sin(n\phi_i}{\sum w_i \cos(n\phi_i}\right) \tag{3.2}$$

where the sum is carried on every selected track i in the sub-event, w_i are weight corrections, n denotes the order of Fourier harmonic expansion, ϕ is the track azimuth angle and Ψ is the reconstructed event plane angle. Event Plane determination is sensitive to a non-uniform acceptance in azimuth angle, so weights are used in ϕ, additionally p_T weights are used to improve the event plane resolution. Other methods to correct for acceptance issues include recentering of the event or event mixing (both not used in this study). It should be noted that the UrQMD model has an event plane angle equal to a constant of zero. For convenience the event plane angle is shifted to positive values *e.g.* $\Psi_1 \in [-\pi;+\pi] \rightarrow \Psi_1 \in [0;2\pi]$ for the first harmonic ($\Psi_2 \in [-\pi/2;+\pi/2] \rightarrow \Psi_2 \in [0;+\pi]$ for the second harmonic), which transforms the UrQMD event plane angle of 0 rad into π rad.

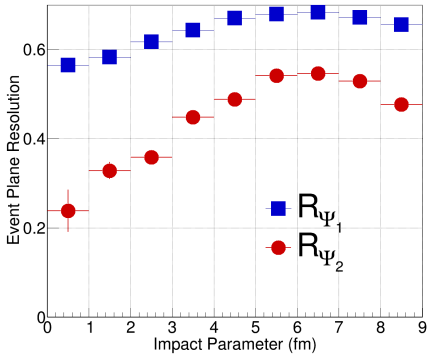

Figure 5: Resolution of the event-plane angle by sub-events versus the impact parameter b

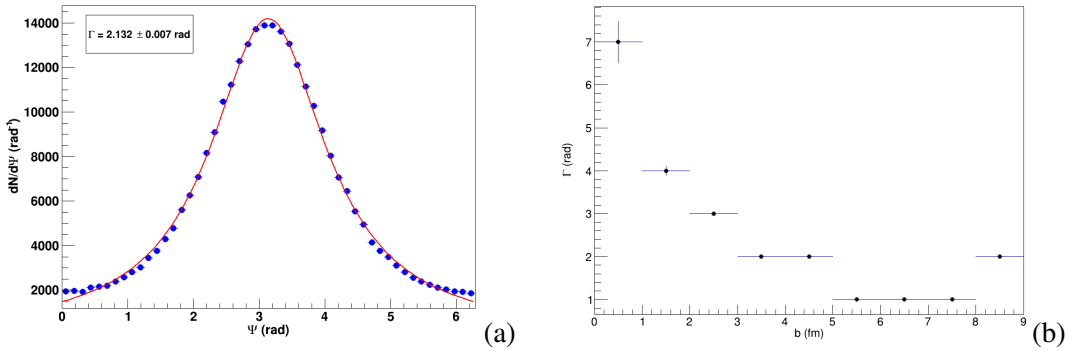

Figure 6: (a) - reconstructed event plane angle Ψ_1, (b) - width of Breit-Wiegner fit Γ versus the impact parameter b

The results were fit with a Breit-Wiegner function as a means of assessing event plane angle estimation versus centrality (impact parameter in this case), as shown in Fig. (6). The event plane resolution over all events is determined by:

$$R_n = \sqrt{2\langle \cos(\Psi_{n,A} - \Psi_{n,B}) \rangle} \tag{3.3}$$

where R_n is the resolution for the n-th harmonic and $\Psi_{A,B}$ are the sub-event plane angles. For this data set the resolution was calculated to be $R_2 = 0.4805 \pm 0.0023$. Resolution of the event-plane angle for the first and second harmonics versus the impact parameter are presentet in Fig. (5). It should be noted that the Zero Degree Calorimeter may provide a complementary role in the event plane determination [7] which is also to be addressed in the future.

3.2 Elliptic Flow of Identified Hadrons

Following the determination of the event plane angle and the corresponding resolution, particles are correlated to the event plane to reveal the observed differential distributions $v_2^{obs}(p_T)$ and $v_2^{obs}(y)$, however they need to be corrected by the event plane resolution to obtain the final results given by $v_2 = v_2^{obs}/R_2$. The integrated elliptic flow coefficient was determined to be $v_2 = 0.0266 \pm 0.0002$ which is in line with measurements made for the elliptic flow versus energy excitation function in several experiments (*e.g.* [8], [9], [10]). It should be noted that the integrated elliptic flow coefficient versus centrality and/or beam energy will also be goals for future studies. On Fig. (7) are shown differential distributions of $v_2(p_T)$ for probability trust thresholds. Misidentification of particles in the higher p_T region is more pronounced, so after applying the $P_{trust} > 0.6$, a more "pure" sample was derived at the cost of statistics, leading to a requirement of a larger data set and further investigation.

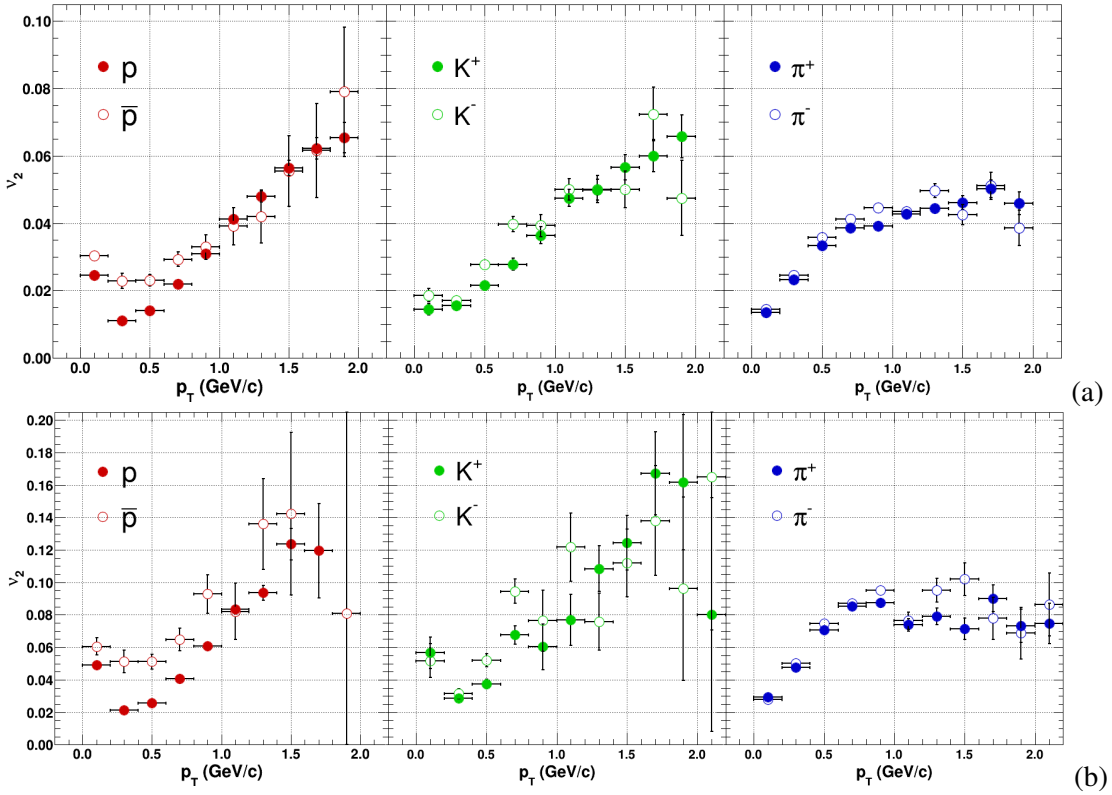

Figure 7: Differential elliptic flow values in bins of transverse momentum, (a) - $P_{trust} > 0$, (b) - $P_{trust} > 0.6$.

3.3 Elliptic Flow of Λ-hyperons

Reconstruction of $\Lambda(\bar{\Lambda})$-hyperons was performed using the decay mode $\Lambda \to p + \pi^-$. The secondary vertex reconstruction utilizes a similar approach to the Kalman filtering formalism described in [24]. For the Λ-hyperon reconstruction the trust probability threshold was not used and tracks were tagged by means of highest probability.

The applied topological cuts are: distance of the closest approach (DCA) of the daughter particles to the primary vertex, small distance of separation in the decay vertex between the tracks, and relatively large decay length of the mother particle. Both the DCA and the two-track separation cuts should have increased efficiency if applied in χ^2-space, *i.e.* when normalized to their respective errors.

The exact values of selection cuts were found by multidimensional scan over the whole set of selection criteria with a requirement to maximize the invariant mass peak significance. It is defined as $S/\sqrt{S+B}$, where S and B are total numbers of signal (described by the gaussian) and background (polynomial function) combinations inside $\pm 2\sigma$ interval around the peak position.

The selection cuts used for this study were optimized for $\sqrt{s_{NN}} = 9$A GeV and it should be noted that better signal to background ratio may be achieved for the $\sqrt{s_{NN}} = 11$A GeV data set used in this study. Moreover, for the flow analysis procedure the signal and background are evaluated in bins of p_T and optimal results can be obtained with further signal to background ratio maximization carried out in these bins.

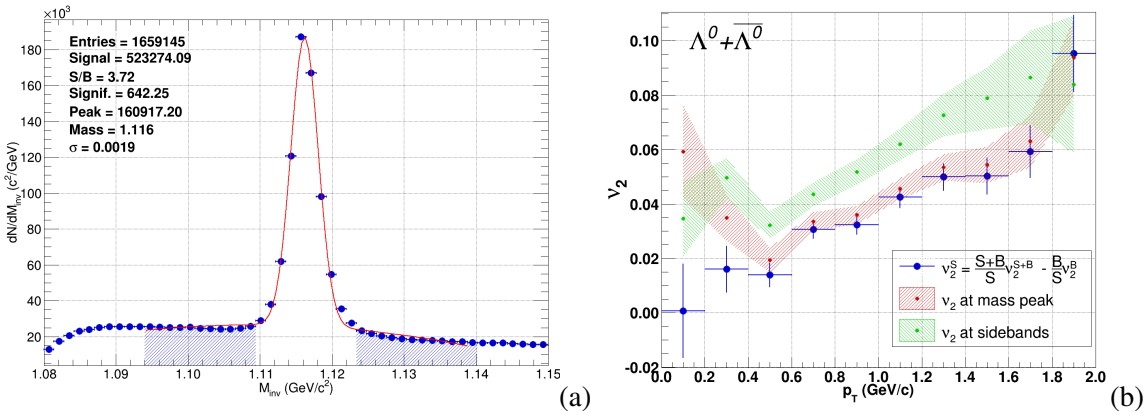

Figure 8: (a) - Invariant mass distribution in bins of 1.4 MeV/c^2 each, (b) - $\Lambda, \bar{\Lambda}$-hyperon elliptic flow

The Λ elliptic flow is evaluated in the invariant mass peak region and in the sidebands region, and the background contribution is removed from the signal by:

$$v_2^S = \frac{S+B}{S} v_2^{S+B} - \frac{B}{S} v_2^B \tag{3.4}$$

where v_2^S is the Λ-hyperon flow "pure" signal, v_2^{S+B} is the flow signal as measured in the mass peak region and v_2^B is the flow signal contribution by the background, measured in the hatched area (see Fig. (8a) [25]. This approach of background subtraction is very straight forward and simple to implement, however, different methods of background subtraction may be added for comparison in further studies. In Fig. (8b) with markers is shown the $v_2(p_T)$ differential flow calculated by (3.4)

and the right and left hatched areas represent the measured flow in the mass peak and sideband regions respectively.

4. Conclusions

A short description of the proposed NICA/MPD project was given. Several points have been made on the prospects of hadron flow studies and the important role hyperons may provide for the better understanding of the initial fireball conditions. Future improvements of the presented results of reconstructed and identified hadrons (p,π,K, Λ) elliptic flow as well as an outlook on subsequent studies in this area of research have been noted.

References

[1] NICA Conceptual Design Report, 2008, *http://nica.jinr.ru/files/NICA_CDR.pdf*.

[2] NICA White Paper, 2011, *http://nica.jinr.ru/files/WhitePaper.pdf*.

[3] MPD Conceptual Design Report, 2011, *http://nica.jinr.ru/files/MPD_CDR_en.pdf*.

[4] V. Kolesnikov and A. Zinchenko for the MPD Collaboration, preprint arXiv:1312.1091v1 [nucl-ex] (2013).

[5] A.Averyanov *et al.*, 2013, *http://nica.jinr.ru/files/MPD/TPC%20TDR-v1_2_1.pdf*

[6] V.Babkin *et al.*, 2009, *http://nica.jinr.ru/files/TOF-MPD.pdf*.

[7] M. B. Golubeva *et al.*, *Physics of Atomic Nuclei*, **76**, p.1-15 (2013).

[8] C. Pinkenburg *et al.*, *Phys. Rev. Lett.* **83**, p. 1295 (1999).

[9] P. Braun-Munzinger, J. Stachel *Nucl. Phys.* **638**, 3c (1998).

[10] H. AppelshÂĺauser *et al.*, *Nucl. Phys.* **698**, 253c (2002).

[11] R. Snellings, preprint arXiv:1102.3010v2 [nucl-ex] (2011).

[12] J. Rafelski and B. Muller, *Phys. Rev. Lett.* **48**, p. 1066 (1982).

[13] F. Antinori *et al.* (WA97 Collaboration), *Eur. Phys. J. C.* **11**, p. 79 (1999).

[14] F. Antinori *et al.* (NA57 Collaboration), *J. Phys. G.* **32**, p. 427 (2006).

[15] L. Adamczyk *et al.* (STAR Collaboration), *Phys. Rev. C.* **88**, 014902 (2013).

[16] S. A. Bass *et al.*, *Prog. Part. Nucl. Phys.* **41**, p. 225-370 (1998).

[17] M. Bleicher *et al.*, *J. Phys. G: Nucl. Part. Phys.* **25**, p. 1859-1896 (1999).

[18] S. Voloshin and Y. Zhang, preprint arXiv:hep-ph/9407282v1 (1994), *Z. Phys. C* **70**, p. 665 (1996).

[19] A. M. Poskanzer and S. Voloshin, preprint arXiv:9805001v2 [nucl-ex] (1998), *Phys. Rev. C* no.CS6346 (1998).

[20] H. Masui and A. Schmah, preprint arXiv:1212.3650v1 [nucl-ex] (2012).

[21] R. Brun *et al.*, *CERN-DD-EE-84-1* (1987).

[22] R. Fruehwirth, *Nucl. Instr. and Meth.* **262**, p.444 (1987).

[23] S.P. Merts *et al.*,*Matem. Mod.* **12**, p. 102 (2012).

[24] R. Luchsinger and Ch. Grab, *Comp. Phys. Comm.* **76**, p. 263 (1993).

[25] C. Bianchin for the ALICE Collaboration, preprint arXiv:1111.6886v1 [hep-ex] (2011).